Journal of ELECTRONIC MATERIALS
DOI: 10.1007/s11664-015-3867-5

Characterization of Copper Oxide Nanoparticles Fabricated by the Sol–Gel Method

ZOHRA NAZIR KAYANI,[1,3] MARYAM UMER,[1] SAIRA RIAZ,[2] and SHAHZAD NASEEM[2]

1.—Lahore College for Women University, Lahore, Pakistan. 2.—Centre of Excellence in Solid State Physics, University of the Punjab, Lahore, Pakistan. 3.—e-mail: zohrakayani@yahoo.com

Copper oxide nanoparticles were successfully prepared by a sol–gel technique. An aqueous solution of copper nitrate $Cu(NO_3)_2$ and acetic acid was used as precursor. On addition of sodium hydroxide (NaOH) a precipitate of copper oxide was immediately formed. The copper oxide nanoparticles were characterized by use of x-ray diffractometry (XRD), thermogravimetric analysis (TGA), differential thermal analysis, differential scanning calorimetry, Fourier-transform infrared spectroscopy (FTIR), vibrating sample magnetometry, and scanning electron microscopy (SEM). The XRD pattern contained sharp peaks of copper oxide nanoparticles with mixed cuprite and tenorite phases. Use of the Debye–Scherer equation showed that the crystallite size of the copper oxide nanoparticles increased with increasing annealing temperature. FTIR spectra revealed vibration of the CuO band at 473 cm^{-1}; a band at 624 cm^{-1} was attributed to Cu_2O. Maximum coercivity and saturation magnetization of the nanoparticles were 276 Oe and 0.034 emu/g, respectively. SEM micrographs of the nanoparticles revealed the presence of spherical nanoparticles of the tenorite phase whereas the cuprite phase was in the form of a compact deposit.

Key words: Nanoparticles, sol–gel, copper oxide, magnetic properties

INTRODUCTION

Cuprous oxide (Cu_2O) is metal-deficient *p*-type semiconductor. It has been reported that growth of cuprous oxide results in formation of two phases, copper(I) oxide Cu_2O and copper(II) oxide CuO, cupric oxide.[1–5] Current applications of copper oxide include use in solar cells and electro-chromic devices.[6] As industrial catalysts, copper oxide nanoparticles may take the place of metal catalysts for oxidation and reduction of carbon monoxide,[7] which minimizes manufacturing costs and enhances catalytic efficiency. Cupric oxide is useful in chemotherapy for patients with acquired immune deficiency syndrome (AIDS). It is also used to produce dry cell and wet cell batteries.[8] A variety of methods have been used to prepare nanoparticles of copper oxides, including sol–gel methods,[9] solid-state reaction,[10] sonochemical preparation,[11] alkoxide-based preparation,[12] glycine-assisted combustion,[13] and a reflux condensation method.[14] Among these techniques the sol–gel technique is easiest, requires use of low temperatures, and is most economical. Nanoparticles of different materials have been synthesized by use of sol–gel techniques.[15–18]

In this study we synthesized copper oxide nanoparticles by use of an inexpensive sol–gel process, and investigated the effect of different annealing temperatures on the structure, microstructure, and magnetic properties of the nanoparticles. Optical properties were indicative of a larger band gap than reported in the literature.[11] This increase in the band gap was because of a quantum size effect. The large band gaps achieved are a novelty of this work.

EXPERIMENTAL

$Cu(NO_3)_2$ was dissolved in deionized water. Acetic acid was mixed with this solution, and the mixture

(Received February 16, 2015; accepted May 22, 2015)

Published online: 04 June 2015

was heated to 100°C with continuous stirring by use of a magnetic stirrer. After continuous stirring for 60 min NaOH was added and a large amount of black precipitate were appeared. The sol was further heated and stirred for 1 h, then aged for 1 day.

Centrifugation was performed at 3000 revolutions/min (rpm), and the bluish green precipitate obtained was transferred to a crucible for annealing. Annealing was performed at 400°C for 4 h, then at 1000°C, by use of a Lindberg/blue furnace. The final product was a black powder which was collected for characterization of the copper oxide nanoparticles.

Powder x-ray diffractometry (XRD) was performed with a Bruker D-8 instrument at a scanning rate of 10°/min from 20° to 80°, with Cu Kα radiation (λ = 1.5406 Å) and a nickel filter. Fourier-transform infrared (FTIR) spectroscopy in the range 4000.00 to 400.00 cm^{-1} was performed with a Midac Corporation M series instrument. The sample and KBr were ground together to produce a pellet. Thermogravimetric analysis was performed with an SDT Q 600. Particle size was evaluated by use of a Malvern Mastersizer-3000 particle-size analyzer. The surface morphology of the nanoparticles was studied by scanning electron microscopy (SEM; S-3400 N; Hitachi).

RESULTS AND DISCUSSION

FTIR

The FTIR spectra of nanoparticles annealed at 400°C contained bands at 473 cm^{-1},[19] 624 cm^{-1}, 1118 cm^{-1}, 1384 cm^{-1}, 1623 cm^{-1}, and 3478 cm^{-1} (Fig. 1). FTIR spectra provide information about the nature of the copper oxide nanoparticles are essential for verifying the purity of the oxide. The band at 473 cm^{-1} was ascribed to CuO vibration whereas that at 624 cm^{-1} was ascribed to Cu_2O. The absorption band at 1118 cm^{-1} was ascribed to NO_3 bending and stretching. The band at 1384 cm^{-1} was ascribed to the C=O bond.[20] Absorption at 1623 cm^{-1} and 3478 cm^{-1} was ascribed to H–O–H bending and O–H stretching respectively.[21] After annealing at 1000°C, the copper oxide peaks became sharper whereas a sharp decrease in intensity was observed for the impurity peaks.

Structural Studies

The crystal structure and phase purity of the nanoparticles were characterized by XRD. For nanoparticles annealed at 400°C, the XRD pattern (Fig. 2) contained two sharp peaks at 2θ = 35.5 and 38.9°, which matched reflections from the (−111) and (111) planes, respectively, of the tenorite structure of CuO.[22,23] A sharp peak at 2θ = 29.4 matched reflections from the (110) plane of the cuprite structure of Cu_2O. For nanoparticles annealed at 1000°C, the XRD pattern (Fig. 2) contained two peaks at 2θ = 35.5° and 38.6° which matched reflections from the (−111) and (111) planes, respectively, of the tenorite structure of CuO. A sharp peak near 2θ = 36.4° matched reflections from the (111) plane of the cuprite structure of Cu_2O. Annealing changed the structure of the copper oxide nanoparticles from cubic to monoclinic structure. Table I shows the XRD data for nanoparticles annealed at 400°C and 1000°C. The XRD patterns confirmed the synthesis of pure, crystalline copper oxide nanoparticles. Two phases, CuO tenorite and Cu_2O cuprite, were confirmed by XRD. The peaks obtained from XRD patterns were in good agreement with JCPDS card 48-1548. No impurity peaks were observed in these XRD patterns.

Average crystallite size (D) was calculated by use of the Scherrer equation, $D = 0.9\lambda/\beta\cos\theta$, where λ was the wavelength of x-ray and β was the full width at half maximum. Table I shows that the crystallite size of tenorite increased from 13.2 nm to 25.1 nm whereas that of cuprite increased from 32.9 mm to 33.5 nm when the nanoparticles were

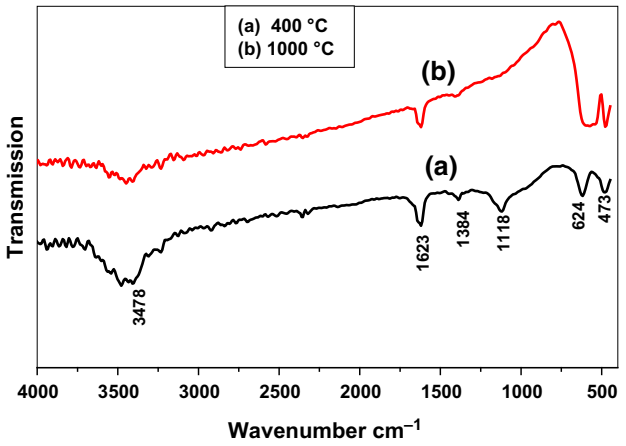

Fig. 1. FTIR spectra of copper oxide nanoparticles annealed at (a) 400°C and (b) 1000°C.

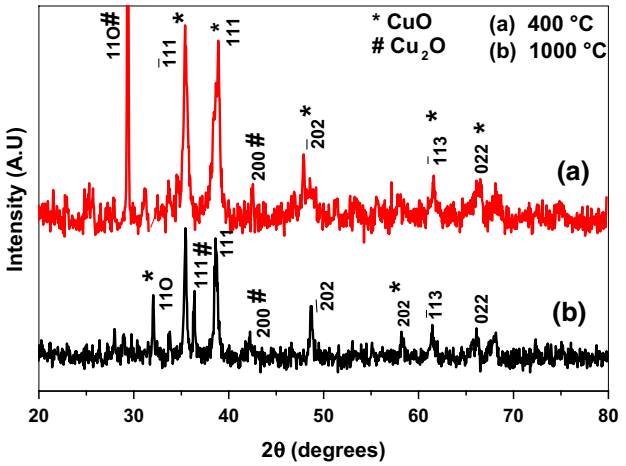

Fig. 2. XRD pattern of copper oxide nanoparticles annealed at (a) 400°C and (b) 1000°C.

Table I. Crystallite size and dislocation density of copper oxide nanoparticles after annealing at different temperatures

Annealing temperatures °C	Crystallite size (nm) CuO tenorite	Crystallite size (nm) Cu_2O cuprite	Dislocation density
400	13.2	32.9	0.01
1000	25.1	33.5	0.008

heated from 400°C to 1000°C. These results showed that as the annealing temperature was increased the crystallite size of copper oxide nanoparticles was increased and broadening of the peaks and dislocation density decreased. Measurement by particle size analysis also showed an increase of particle size from 35.6 nm to 43.2 nm on annealing.

TGA/DTA and DSC

Results from thermogravimetric analysis (TGA), differential thermal analysis (DTA), and differential scanning calorimetry (DSC) are shown in Fig. 3. When the as-prepared nanoparticles were heated, the TG curve revealed weight losses in two broad stages. The first, between 80°C and 140°C, was associated with removal of water from OH groups, the second, between 600°C and 880°C, with decomposition of $Cu_2(OH)_3NO_3$. Figure 3 shows three endothermic peaks at 103°C, 765°C, and 905°C and three exothermic peaks at 115°C, 790°C, and 920°C in the DSC plot. The endothermic peak at 103°C might be because of dehydration of the precursor. The two endothermic peaks at 765°C and 905°C were because of decomposition of $Cu(NO_3)_2$ to copper(lI) oxide. The exothermic peak at 920°C might be because of crystallization of amorphous, dehydrated copper oxide.[24] The DTA plot contained two main peaks, an endothermic peak at 920°C and an exothermic peak at 935°C. Under linearly increasing temperature conditions the dehydration process indicated an anomaly in the DSC curve. The exothermic peak in the DTA curve was ascribed to crystallization of the amorphous dehydrated product whereas the endothermic peak was ascribed to decomposition of $Cu_2(OH)_3NO_3$.

Optical Properties

Variation of the percentage transmission of copper oxide nanoparticles as a function of wavelength is shown in Fig. 4. Transmission spectra were used to study the effect of annealing temperature on band gap energies of the copper oxide nanoparticles. To estimate the value of the optically wide band gap of copper oxide nanoparticles from the transmission spectra, the wavelength at which transmission abruptly changed was recorded. This was 367 nm and 350 nm for nanoparticles annealed at 400°C and 1000°C, respectively. The band gap of the copper oxide nanoparticles annealed at 400°C was calculated to be 3.38 eV from the UV–visible transmission spectrum; annealing at 1000°C increased the band gap to 3.54 eV, which was larger than that reported for bulk CuO (E_g = 1.85 eV).[25] Light absorption occurred at 367 nm and 350 nm for nanoparticles annealed at 400°C and 1000°C, respectively. This absorption led to an electron in the conduction band and a hole in the valence band. Nanoparticle energy was confined to potential wells with small lateral dimensions, and the energy difference between the positions of the conduction band and the free electron gave information about quantization of energy levels. This phenomenon occurs when the size of the nanoparticles becomes comparable with the de Broglie wavelength of a charge carrier. The increase in the band gap of the annealed copper oxide nanoparticles was a consequence of quantum size effects.[26]

Magnetic Properties

Basic magnetic characterization was performed for copper oxide nanoparticles annealed at 400°C and 1000°C. Figure 5 shows the M (H) (hysteresis) behavior of air-annealed samples of copper oxide nanoparticles.

The saturation magnetization (M_S), remnant magnetization (M_r), square-ness ratio (S^*) and the coercivity (H_c) were determined by interpreting the magnetic hysteresis loop at room temperature. All air-annealed samples of copper oxide nanoparticles had a magnetic response up to the maximum applied field, with maximum saturation magnetization 0.034 emu/g. Table II shows that coercivity decreased from 276 Oe to 47 Oe when the annealing temperature was increased from 400°C to 1000°C whereas saturation magnetization increased from 0.0022 emu/g to 0.034 emu/g. Squareness ratio had small values ranging from 0.089 to 0.032. This trend was observed for ferromagnetic nanoparticles, for which magnetization was observed to increase with increasing particle size.[27,28] XRD study showed an increase in crystallite size with increasing annealing temperature. The magnetic measurements showed presence of a ferromagnetic (FM) component with maximum coercivity of 276 Oe and maximum saturation magnetization of 0.034 emu/g. For ferromagnetic nanoparticles, the magnetic moment corresponded to the core of the particle and the surface spin behaved as a disordered collection of spins. Therefore, a decrease in particle size increased the surface to volume ratio, hence reduc-

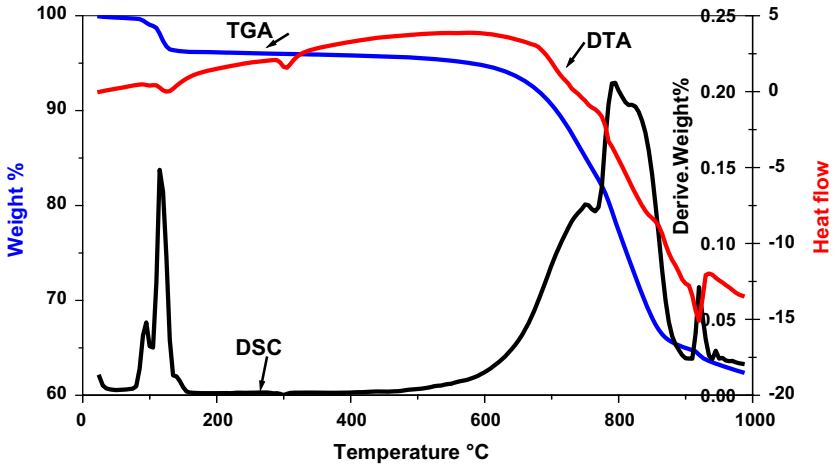

Fig. 3. TGA/DTA and DSC curves for copper oxide nanoparticles.

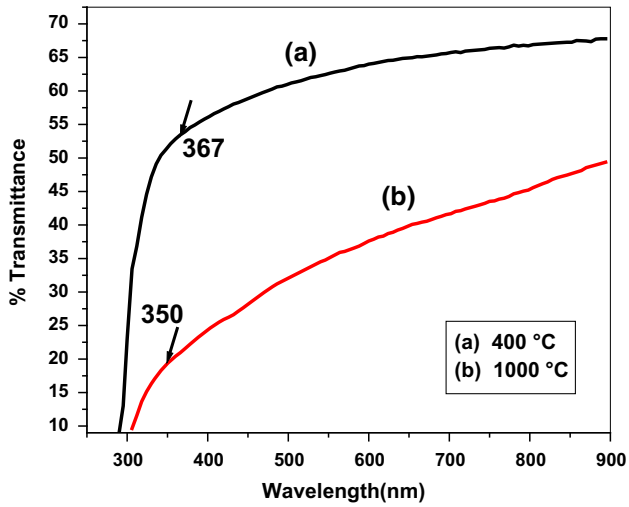

Fig. 4. Transmission spectra of copper oxide nanoparticles annealed at (a) 400°C and (b) 1000°C.

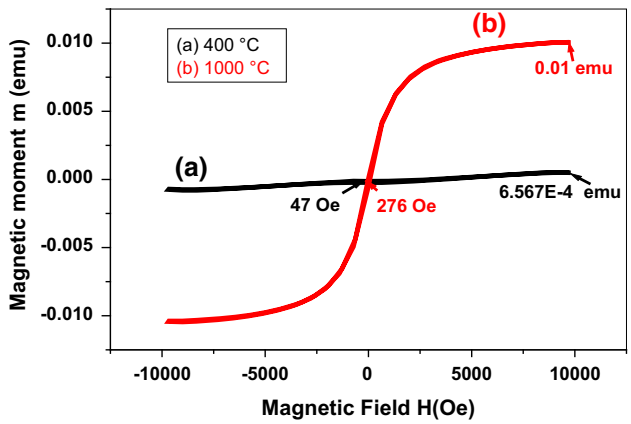

Fig. 5. Magnetic hysteresis of copper oxide nanoparticles annealed at (a) 400°C and (b) 1000°C.

ing the net magnetization. The oxygen vacancies not only imparted a moment on the metal ions but also supplied charge carriers for mediating the ferromagnetism between the canted Cu spin. These charge carriers were responsible for ferromagnetic interactions between the uncompensated surface spins of CuO nanoparticles. The origin of ferromagnetism was because of different valence states of copper ions, because of the presence of oxygen vacancies at the surface or interface of the nanoparticles. This resulted in exchange interactions between localized electron spin moments, because of oxygen vacancies at the surfaces of the nanoparticles.[29,30] Table II shows that with increasing annealing temperature from 400°C to 1000°C, crystallite size and saturation magnetization of nanoparticle increased whereas coercivity was decreased. This means annealing oriented all the domains in one direction, resulting in the formation of soft magnetic nanoparticles.

Surface Morphology

Synthesis of copper oxide nanoparticles furnished Cu_2O or CuO phases at 400°C and 1000°C. The morphology of the copper oxide nanoparticles was examined by SEM (Fig. 6). It was apparent from the SEM image that the tenorite particles were spherical in shape and that interconnection of a multigranular structure led to greater porosity than for cuprite, which was in the form of pyramid aggregates which resulted in a compact material. Similar surface morphology of copper oxide nanoparticles has also been reported in the literature.[24,31,32] Nanoparticles agglomerated during heating (Fig. 6b). Comparison of the morphology of nanoparticles annealed at 400°C and 1000°C (Fig. 6a and b) revealed that the shape of copper oxide nanostructures could be modified by changing the temperature. Annealing led to the formation of

Table II. Magnetic properties of copper oxide nanoparticles

Annealing temperature (°C)	Coercivity H_c (Oe)	Magnetic moment m_s (emu)	Saturation magnetization M_S (emu/g)	Remanent magnetization M_r (emu/g)	Squareness ratio $S^* = M_r/M_S$
400	276	6.567E−4	2.189E−3	1.939E−4	0.0886
1000	47	0.01	0.034	1.095E−3	0.032

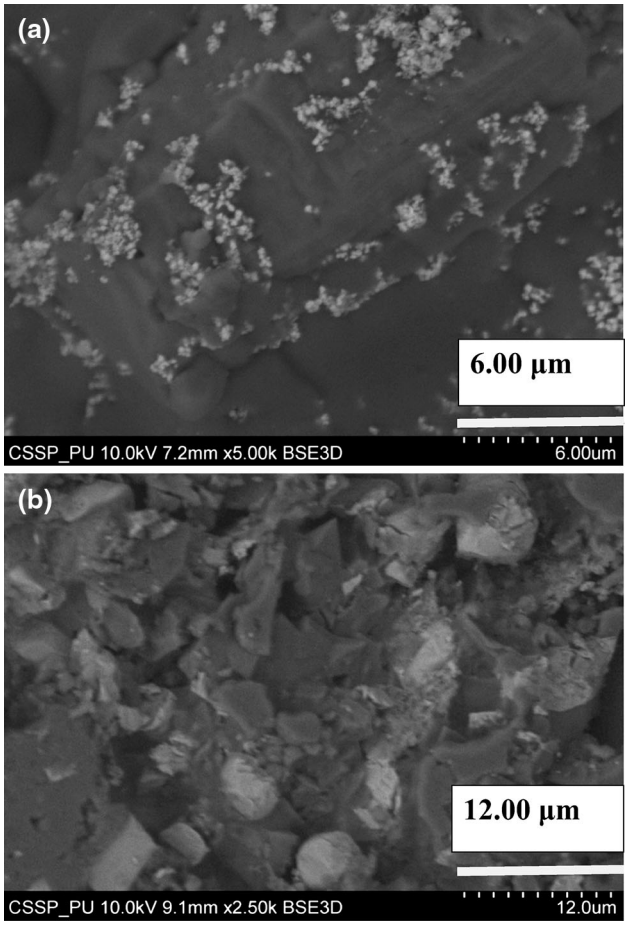

Fig. 6. Surface morphology of copper oxide nanoparticles annealed at (a) 400°C and (b) 1000°C.

larger grains by coalescence of smaller grains, which increased the crystallinity of the nanoparticles.

CONCLUSIONS

Copper oxide nanoparticles with mixed tenorite and cuprite phases were successfully prepared by a sol–gel method. After annealing at 400°C crystallite size was 13.2 nm for tenorite and 32.1 nm for curite; this was increased by annealing at 1000°C. Annealing changed the cubic structure of copper oxide nanoparticles to the monoclinic structure. A clear hysteresis loop was observed for the nanoparticles. Annealing of CuO nanoparticles at different temperatures showed that oxygen vacancies at the surface of the particles were responsible for the ferromagnetism. Such ferromagnetism without presence of any transition metal could be used in spintronics.

REFERENCES

1. V. Saravanan, P. Shankar, G.K. Mani, and J.B.B. Rayappan, *J. Annal. Appl. Pyrol.* 11, 272 (2015).
2. O. Messaoudi, H. Makhlouf, A. Souissi, I.B. Assaker, M. Karyaoui, A. Bardaoui, M. Oueslati, and R. Chtourou, *J. Alloys Compd.* 611, 142 (2014).
3. M.R. Johan, M. Shahadan, M. Suan, N.L. Hawari, and H.A. Ching, *Int. J. Electrochem. Sci.* 6, 6094 (2011).
4. P. Mallick, *Proc. Natl. Acad. Sci., India, Sect. A* 84, 387 (2014).
5. K.H. Yoon, W.J. Choi, and D.H. Kang, *Thin Solid Films* 372, 250 (2000).
6. T.J. Richardson, J.L. Slack, and M.D. Rubin, *Appl. Phys. Lett.* 98, 262 (2000).
7. K. Zhou, R. Wang, B. Xu, and Y. Li, *Nano-technology* 17, 3939 (2006).
8. G. Joseph and J.A. Kundig, *Copper: Its Trade, Manufacture, Use and Environmental Status* (Materials Park, OH: ASM International, 1999).
9. R. Etefagh, E. Azhir, and N. Shahtahmasebi, *Sci. Iran. F* 20, 1055 (2013).
10. J.F. Xu, W. Ji, Z.X. Shen, S.H. Tang, X.R. Ye, D.Z. Jia, and X.Q. Xin, *J. Solid State Chem.* 147, 516 (2000).
11. R.V. Kumar, Y. Diamant, and A. Gedanken, *Chem. Mater.* 12, 2301 (2000).
12. C.L. Carnes, J. Stipp, and K.J. Klabunde, *Langmuir* 18, 1352 (2002).
13. O.H. Abd-Elkader and N.M. Deraz, *Int. J. Electrochem. Sci.* 8, 8614 (2013).
14. N. Bouazizi, R. Bargougui, A. Oueslati, and R. Benslama, *Adv. Mater. Lett.* 6, 158 (2015).
15. S. Devi and M. Srivastva, *Ind. J. Phys.* 84, 1561 (2010).
16. M. Riazian, *Ind. J. Phys.* 87, 991 (2013).
17. Z.N. Kayani, S. Arshad, S. Riaz, and S. Naseem, *IEEE Trans. Magn.* 50, 2200404 (2014).
18. Z.N. Kayani, F. Saleemi, and I. Batool, *Appl. Phys. A* (2015). doi:10.1007/s00339-015-9019-1.
19. S. Srivastava, M. Kumar, A. Agrawal, and S. Dwivedi, *IOSR-JAP* 5, 61 (2013).
20. S.S. Alias, A.B. Ismail, and A.A. Mohamad, *J. Alloys Compd.* 499, 231 (2010).
21. M. Ohanishi, A. Kusachi, S. Kobayashi, and J. Yamakawa, *J. Miner* 102, 233 (2007).
22. E. Darezereshki and F. Bakhtiari, *J. Min. Metall. Sect. B* 49, 21 (2013).
23. Z. Endut, M. Hamdi, and W.J. Basirun, *Thin Solid Films* 528, 213 (2013).
24. E. Darezereshki and F. Bakhtiari, *J. Min. Metall. Sect. B* 47, 73 (2011).
25. K. Santra, C.K. Sarkar, M.K. Mukherjee, and B. Cosh, *Thin Solid Films* 213, 226 (1992).
26. J.P. Yang, F.C. Meldrum, and J.H. Fendler, *J. Phys. Chem.* 99, 5500 (1995).
27. K. Maaz, A. Mumtaz, K.S. Hasanain, and A. Cylan, *J. Magn. Magn. Mater.* 308, 289 (2007).

28. S. Rehman, A. Mumtaz, and S.K. Hasanain, *J. Nanopart. Res.* 13, 2497 (2011).
29. J.W. Chen and G.N. Rao, *IEEE Trans. Magn.* 47, 3772 (2011).
30. D. Gao, J. Zhang, J. Zhu, J. Qi, Z.I. Zhang, W. Sui, H. Shi, and D. Xue, *Nanoscale Res. Lett.* 5, 769 (2010).
31. C. Maccato, Q. Simon, G. Carraro, D. Barreca, A. Gasparotto, O.I. Lebedev, S. Turner, and G.V. Tendeloo, *J. Adv. Microsc. Res.* 7, 84 (2012).
32. N. Kumaresan, K. Ramamurthi, S. Mathuri, M.M.A. Sinthiya, T. Manimozhi, M.M. Margoni, and R. Rameshbabu, *Int. J. Chem. Tech Res.* 7, 1598 (2015).